



Dipole Fluctuation and Structural Phase Transition in Hydrogen-Bonding Molecular Assemblies of Mononuclear Cu^{II} Complexes with Polar Fluorobenzoate Ligands

Journal:	<i>Dalton Transactions</i>
Manuscript ID	DT-ART-06-2021-002118.R1
Article Type:	Paper
Date Submitted by the Author:	05-Aug-2021
Complete List of Authors:	Takahashi, Kiyonori; Hokkaido University, Research Institute for Electronic Science; Hokkaido University, Graduate School of Environmental Science Miyazaki, Yuji; Osaka University, Research Center for Structural Thermodynamics, Graduate School of Science Noro, Shin-ichiro; Hokkaido University, Faculty of Environmental Earth Science Nakano, Motohiro; Osaka Univ., Nakamura, Takayoshi; Hokkaido University, Research Institute for Electronic Science Akutagawa, Tomoyuki; Tohoku University, Institute of Multidisciplinary Research for Advanced Materials

ARTICLE

Received 00th January
20xx,

Dipole Fluctuation and Structural Phase Transition in Hydrogen-Bonding Molecular Assemblies of Mononuclear Cu^{II} Complexes with Polar Fluorobenzoate Ligands

Accepted 00th January 20xx

Kiyonori Takahashi,^{*a} Yuji Miyazaki,^b Shin-ichiro Noro,^c Motohiro Nakano,^b Takayoshi Nakamura,^a and Tomoyuki Akutagawa^{d*}

DOI: 10.1039/x0xx00000x

A series of mononuclear Cu^{II} complexes, [Cu^{II}(4-FBA)₂(py)₂(H₂O)] (**1**), [Cu^{II}(3-FBA)₂(py)₂(H₂O)] (**2**), and [Cu^{II}(3,4-F₂BA)₂(py)₂(H₂O)] (**3**), where 4-FBA = 4-fluorobenzoate, 3-FBA = 3-fluorobenzoate, 3,4-F₂BA = 3,4-difluorobenzoate, and py = pyridine, respectively, was synthesized and the complexes crystallographically identified. All the Cu^{II} complex crystals share a one-dimensional O–H•••O hydrogen-bonding chain substructure, although the mutual alignment of fluorinated benzoate (F_xBA) ligands exhibits subtle differences among the various compounds, i.e., F_xBA ligands align in an antiparallel fashion in crystals **1** and **3**, while 3-FBA ligands in crystal **2** are interdigitated with a tilt along the *a* axis. Reversible phase transitions were found upon heating at 170.7, 171.3, and 267.5 K for crystals **1**, **2**, and **3**, respectively; all crystals showed approximately 3% expansion and shrinkage of the intermolecular O–H•••O hydrogen bond distances associated with the thermally activated orientational fluctuations of the F_xBA ligands in crystals **1** and **3**. The increase in dielectric constant with increasing temperature, at 240 K, activated molecular fluctuation in the 3,4-F₂BA ligands in crystal **3**. Heat capacity measurements indicated that both the expansion and shrinkage of hydrogen bonds, and the molecular fluctuation in 3,4-F₂BA ligands, contributed to phase transition, and the latter caused dipole fluctuation, resulting in a dielectric anomaly in crystal **3**.

Introduction

Crystal engineering utilizes various types of intermolecular interactions, such as electrostatic, charge-transfer, hydrogen-bonding, and dipole–dipole interactions, to design and control the molecular assembly structures and their physical functions,^{1–7} and it is a promising technology for fabricating semiconducting,² metallic,³ superconducting,⁴ magnetic,⁵ ferroelectric,⁶ and nonlinear optical molecular materials.⁷ Dynamic functional molecular materials exhibiting thermally activated structural motion have attracted much attention because of potential abilities to switch physical functions through molecular motions in the solid state.^{8–10} Molecular

motions within a crystal particularly affect the dielectric response through dipole inversion and fluctuation. The ferroelectric transition due to the flip-flop motion of the supramolecular cation has been observed in the (3-FAni⁺)(DB[18]crown-6)[Ni(dmit)₂]⁻ crystal (where 3-FAni⁺ and DB[18]crown-6 are 3-fluoroanilinium and dibenzo-18-crown-6, respectively).¹¹ The cooperative dipole inversion of the polar 3-FAni⁺ cations along the C–NH₃⁺ axis caused the ferroelectric–paraelectric phase transition around 350 K. In efforts to realize molecular motion in crystals, metal–organic frameworks (MOFs) are considered to be suitable materials, where functional responses are readily designed by replacing the metal ions and ligands. The two-fold motion of the phenylene ring in the three-dimensional (3D) robust network of [Zn₄O(BDC)₃] (well-known as MOF-5, where BDC²⁻ = 1,4-benzodicyclohexadiene-2,5-dicarboxylate²⁻) was observed with an energy barrier of ~ 11.3 ± 2 kcal mol⁻¹.¹² To enhance dielectric response, a motional unit should interact with another within moderate distances in a close-packed crystal in such a way that the unit can accommodate for the motion. We focused on the directional intermolecular interactions between ligands in metal complexes. The highly directional intermolecular interaction can form an assembly structure, which has the possibility of retaining the motional space through weak interactions. Among the variety of directional intermolecular interactions, we have focused on the combination between hydrogen bonding and dipole–dipole interaction.^{13–15} In the

^a Research Institute for Electronic Science, Hokkaido University, Sapporo 001-0020, Japan

^b Research Center for Thermal and Entropic Science, Graduate School of Science, Osaka University, Toyonaka, 560-0043, Japan

^c Faculty of Environmental Earth Science, Hokkaido University, Sapporo, 060-0810 Japan

^d Institute of Multidisciplinary Research for Advanced Materials, Tohoku University, Sendai 980-8577, Japan.

E-mail: (KT) ktakahashi@es.hokudai.ac.jp, (TA) akutagawa@tohoku.ac.jp

Electronic Supplementary Information (ESI) available: Differential scanning calorimetry, changes in x-ray oscillation photographs, crystallographically independent molecular structures with atomic numbering at various temperatures, summary of hydrogen–bonding distance, temperature– and frequency–dependent dielectric constant (ϵ_1) for crystal **1** and **2**, and potential energy curve for F_xBA ligand rotation by DFT calculation.. See DOI: 10.1039/x0xx00000x

present study, we utilized $[\text{Cu}-\text{H}_2\text{O}\cdots(-\text{OOC})_2-\text{Cu}]$ -type hydrogen bonding interaction to synthesize $[\text{Cu}^{\text{II}}(4\text{-FBA})_2(\text{py})_2(\text{H}_2\text{O})]$ (**1**), $[\text{Cu}^{\text{II}}(3\text{-FBA})_2(\text{py})_2(\text{H}_2\text{O})]$ (**2**), and $[\text{Cu}^{\text{II}}(3,4\text{-F}_2\text{BA})_2(\text{py})_2(\text{H}_2\text{O})]$ (**3**), where 4-FBA = 4-fluorobenzoate, 3-FBA = 3-fluorobenzoate, 3,4-F₂BA = 3,4-difluorobenzoate, and py = pyridine. Although crystal structure of **1** at room temperature was reported,¹⁵ dynamic behavior of **1** has not been investigated. Cu^{II} complexes of **2** and **3** were newly synthesized with expectation that complexes of **2** and **3** should be aligned one-dimensionally by hydrogen bonding. To realize dipole–dipole interaction between one-dimensional (1D) chain, we introduced three fluorinated benzoates (F_xBAs) as ligand. Because fluorine (F) atoms induce a strong dipole moment, anisotropic arrangement of ligands through dipole–dipole interactions is expected to modulate the molecular assembly structures and different position of F atom in F_xBA ligands should induce different dipolar interaction between the ligands. Furthermore, the relatively small size of the F atom may be advantageous for molecular motion.¹¹ Herein, we report the dynamic structure and dielectric properties of crystals **1–3**, associated with the phase transition behavior. We have found that the F atom at 4-position of 3,4-F₂BA ligand in crystal **3** has an important role in making a suitable alignment for the fluctuation of 3,4-F₂BA ligand, inducing dielectric anomaly by the dipole fluctuation of F atom at 3-position of 3,4-F₂BA ligand. These characteristics in crystal **3** have been clarified based on the comparison with the structures and physical properties of the crystals **1** and **2**.

Experimental

Preparation of complexes.

Commercially available chemical reagents were used, without further purification, for the syntheses and crystal growth. Cu^{II}(acetate)₂•(H₂O) (1.1×10^{-3} mol) and corresponding

fluorinated benzoic acids (2.7×10^{-3} mol) were refluxed in a mixed solvent system: H₂O (10 mL)/py (2 mL). A further quantity of py was slowly added until the respective mixtures were fully dissolved. The reaction mixtures were held at 283 K for one week, whereafter crystalline samples were obtained. The formulae of complexes **1**, **2**, and **3** were determined to be as follows, based on results of elemental analysis and single-crystal X-ray analysis: $[\text{Cu}(4\text{-FBA})_2(\text{py})_2(\text{H}_2\text{O})]$, $[\text{Cu}(3\text{-FBA})_2(\text{py})_2(\text{H}_2\text{O})]$, and $[\text{Cu}(3,4\text{-F}_2\text{BA})_2(\text{py})_2(\text{H}_2\text{O})]$, respectively. Elemental analysis results: **1**: Calcd. for C₂₄H₂₀O₅N₂CuF₂: C, 55.65%; H, 3.89%; N, 5.41%. Found: C: 55.59%, H: 3.98%, N: 5.47%, **2**: Calcd. for C₂₄H₂₀O₅N₂CuF₂: C, 55.65%; H, 3.89%; N, 5.41%. Found: C: 55.33%, H: 4.02%, N: 5.45%, and **3**: Calcd. for C₂₄H₁₈O₅N₂CuF₄: C, 52.04%; H, 3.28%; N, 5.06%. Found: C: 51.91%, H: 3.40%, N: 5.10%.

Thermal analysis.

Differential scanning calorimetry (DSC) was conducted using a Mettler Toledo DSC 1 STAR[®] system (reference empty Al pan) under a N₂ gas flow in the temperature range 150–330 K. The scan and N₂ flow rates were 5 K min⁻¹ and 40 mL min⁻¹, respectively. Adiabatic heat capacity measurements were carried out with a handmade adiabatic calorimeter,¹⁶ and according to a previously reported procedure.¹⁶ Sample weights of crystals **1**, **2**, and **3** were 0.23049, 0.17533, and 0.17619 g, respectively.

X-ray crystal structure analysis.

Thin polyimide films (MiTeGen MicroMounts) were used for the mounting of each crystal with Paratone oil (Hampton Research Parabar 10312). Temperature-dependent crystallographic data (Table 1) were collected using a Rigaku RAPID-II diffractometer equipped with a rotating anode, fitted with a multilayer confocal optic, using Cu-K_α ($\lambda = 1.54187$ Å) radiation. Calculations were performed using crystal structure software packages (Rigaku Corp.), and olex2¹⁷ only for crystal **1**

Table 1. Crystal data, data collection, and reduction parameter for crystals **1**, **2**, and **3** at various temperatures.

	1 (300 K) ^a	1 (160 K)	2 (250 K)	2 (100 K)	3 (300 K)	3 (240 K)
Ligand	4-FBA	4-FBA	3-FBA	3-FBA	3,4-F ₂ BA	3,4-F ₂ BA
Space group	C2/c (#15)	C2/c (#15)	Fdd2 (#43)	Fdd2 (#43)	C2/c (#15)	C2/c (#15)
<i>a</i> , Å	15.9217(3)	15.8640(3)	15.7319(6)	46.1982(10)	16.0191(7)	49.7886(15)
<i>b</i> , Å	6.0716(1)	29.7886(6)	46.3383(14)	46.8472(10)	6.1375(3)	6.11641(18)
<i>c</i> , Å	23.7095(5)	23.6221(6)	6.1947(2)	6.0941(11)	23.9290(11)	40.4687(14)
α , deg	-	-	-	-	-	-
β , deg	92.1815(9)	92.2320(10)	-	-	92.110(3)	109.524(2)
γ , deg	-	-	-	-	-	-
<i>V</i> , Å ³	2290.34(8)	11154.5(4)	4515.9(3)	13189(2)	2351.04(18)	11636.2(6)
<i>T</i> , K	300	160	250	100	300	240
<i>Z</i>	4	20	8	24	4	4
<i>D</i> _{calc} , g·cm ⁻³	1.502	1.539	1.524	1.565	1.565	1.581
μ , (Cu-K α) cm ⁻¹	18.351	18.33	18.615	19.12	19.57	19.771
Reflections measured	18057	62172	11863	29453	11758	58302
Independent reflections	2102	10209	2064	5918	2147	10643
Reflections used	2102	10209	2064	5918	2147	10643
<i>R</i> _{int}	0.0724	0.0974	0.0337	0.0745	0.0474	0.0698
<i>R</i> ₁ ^a	0.0570	0.1481	0.0395	0.1084	0.0480	0.0630
<i>R</i> _w (<i>F</i> ²) ^b	0.1848	0.2804	0.1077	0.2374	0.1279	0.1701
GOF	1.121	1.050	0.950	1.055	1.006	0.738
Flack parameter	-	-	-0.037(17)	0.031(17)	-	-

^a Data of crystal **1** at 300 K were already published in reference.¹⁵ ^b $R_1 = \sum ||F_o| - |F_c|| / \sum |F_o|$ and $R_w = (\sum w(|F_o| - |F_c|)^2 / \sum wF_o^2)^{1/2}$.

at 160 K. Initial structures were solved using SIR2004,¹⁸ SIR2011,¹⁹ and SHELXT,²⁰ structural refinement was performed using SHELXL 2013.²¹ Parameters were refined using anisotropic temperature factors, except in the case of the hydrogen atoms. Crystal structure of **1** at 300 K were referenced from the literature to compare with the structure of **1** at 160 K.¹⁵ These structural data are provided free of charge by The Cambridge Crystallographic Data Centre. CCDC-1968682, 1968683, 1968684, 1968685 and 1968686 for **1** at 160 K, **2** at 300 K, **2** at 100 K, **3** at 300 K and **3** at 240 K, respectively.

Temperature- and frequency-dependent dielectric constants.

The temperature- and frequency-dependent dielectric constants (ϵ_1) were measured using the two-probe AC impedance method, from 1 kHz to 1 MHz (Hewlett-Packard, HP4194A), and the temperature controller of a Linkam LTS-E350 system. To apply an electric field, samples were molded to pellets (ϕ 3 mm) using a tablet-molding apparatus (STJ-0128, S.T. Japan). The electrical contacts were prepared using silver paste (Dotite D-550) for crystals **1** and **2**, and carbon paste (Dotite XC-12) for crystal **3**, to attach the 25- μm ϕ gold wires to each pellet.

Results and discussion

Coordination geometry and hydrogen-bonding network above the phase transition temperature.

Figures 1a and 1b summarize the 1D hydrogen-bonding chains of Cu^{II} coordination units and the two-dimensional (2D) network assembly of the 1D chains in crystal **1**, similar to in crystals **2** and **3**. Two 4-FBA and two py ligands are coordinated to a Cu^{II} center to form an almost planar O₂N₂ tetra-coordination geometry, where one further H₂O molecule is coordinated at the axial site to form a penta-coordinated Cu^{II} geometry of Cu–O₃N₂ (Figure 1a). Each mononuclear Cu^{II} penta-coordination unit was interacted through the effective intermolecular O–H...O hydrogen-bonding interaction between an axial H₂O ligand and the free O atom of the carboxylate group, forming the 1D chain along the *b* axis. Furthermore, each chain assembled to form a 2D network layer via the weak C–H...O intermolecular interaction between py and the free O atom of the carboxylate group. Orientational disorder of 3,4-F₂BA ligands was observed in crystal **3** at the two independent **A** and **B** sites, with 0.5:0.5 occupancy (Figure 1c), where the disordered F atoms at the 3-position of the 3,4-F₂BA ligand were observed at the four independent sites, each with an occupancy of 0.25, while those at the 4-position were observed at two sites, with 0.5:0.5 occupancy.

Although the formation of 1D hydrogen-bonding chains and weakly interacted 2D layers were the common structural features in crystals **1**, **2**, and **3**, the 3D packing structures were different to each other. Figure 2 summarizes the packing structure and schematic orientation of F_xBA ligands between the nearest neighboring chains. The 4-FBA and 3,4-F₂BA

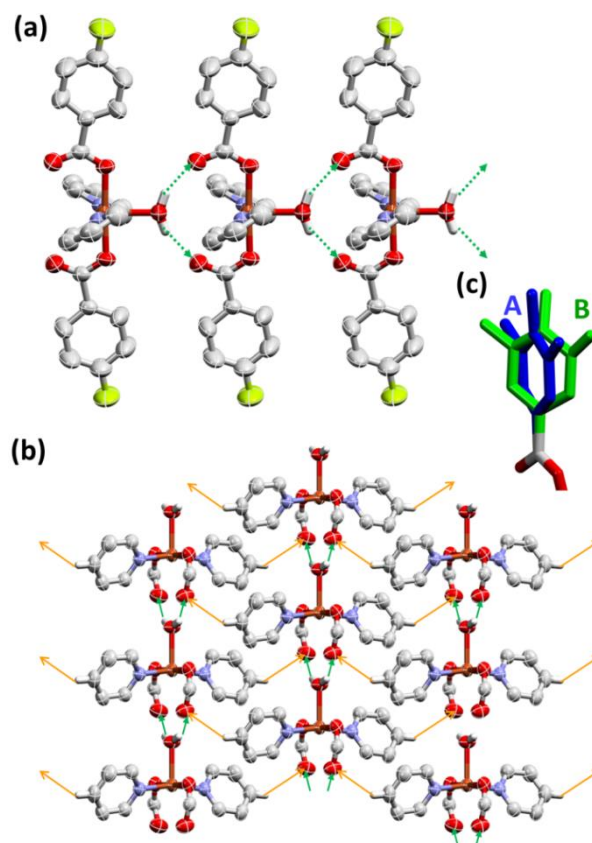


Figure 1. Crystal structures of Cu^{II} complexes of **1** and **3** at 300 K. Hydrogen atoms on 4-FBA and py are omitted for clarity. (a) The 1D O–H...O hydrogen-bonding chain of the penta-coordinated mononuclear Cu^{II} complex in crystal **1**, where the free oxygen atom of 4-FBA ligand and H₂O ligand connect each Cu^{II} complex along the *b* axis. (b) Weakly bonded 2D network structure, via the intermolecular C–H...O interaction between py ligands and free oxygen atom of 4-FBA ligands in crystal **1**. Yellow and green arrows correspond to the O–H...O and C–H...O interactions, respectively. Phenyl rings in 4-FBA ligands are omitted for clarity. (c) Orientational disorder of 3,4-F₂BA ligands in crystal **3**, where the blue and green molecular structures correspond to the **A** and **B** sites, respectively.

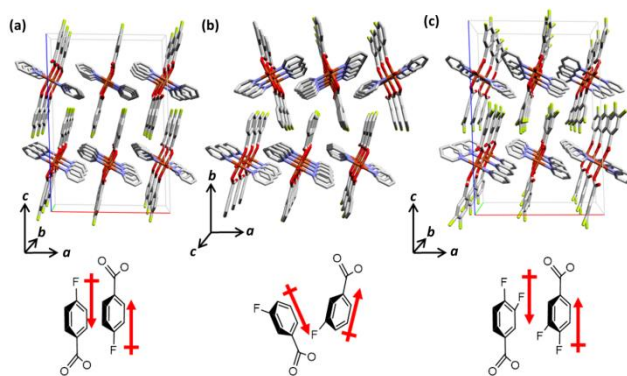


Figure 2. Packing structures of the 1D hydrogen-bonding chains in crystals (a) **1**, (b) **2**, and (c) **3**, viewed along the *b*, *c*, and *b* axes, respectively (upper figures). The disordered B site of the 3,4-F₂BA ligand in crystal **3** is omitted for clarity. Schematic orientation of two F_xBA ligands which are the nearest neighbors and the arrangement of the dipole moments along the C–COO[−] axis of the F_xBA ligand (lower figures).

ligands in crystals **1** and **3** are arranged almost parallel to each other, cancelling the dipole moment of the F atoms at the 4-position (Figures 2a and 2c). In crystal **2**, the π -planes are not parallel, tilted along the [100] or $[\bar{1}00]$ direction. The difference in polar ligand orientation between the nearest neighboring 1D hydrogen-bonding chains was dominated by the substituted position of the F atom, where the dipole-

dipole interaction played an important role in the formation of the 3D packing structure.

dependent structural modulation in the 1D hydrogen-bonding interactions were also affected by the orientational changes of

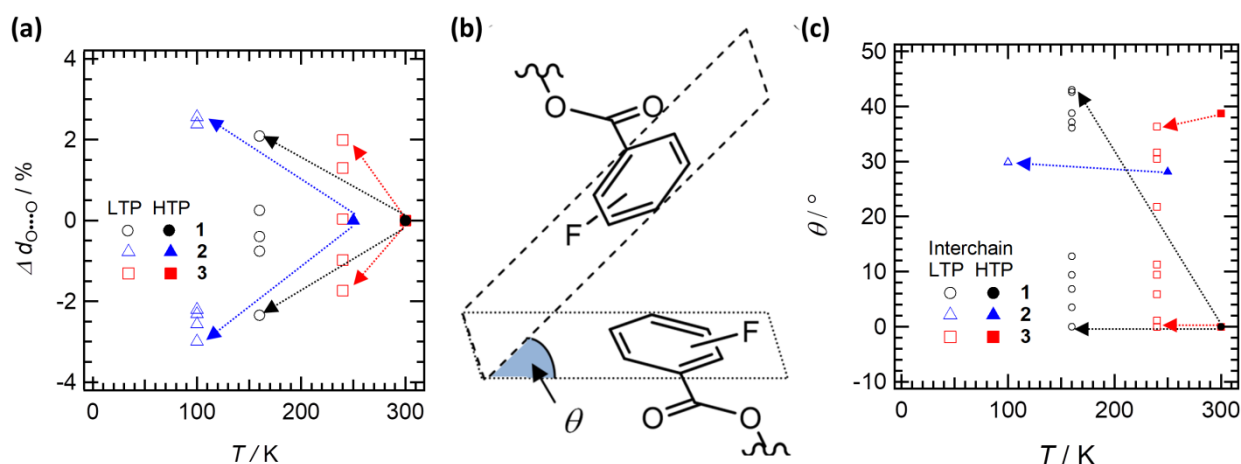


Figure 3. Temperature-dependent structural transformation across the phase transitions. Circle, triangle, and square symbols correspond to crystals **1**, **2**, and **3**, respectively, where the filled and open symbols are the structural parameters of the high temperature phase (HTP) and low temperature phase (LTP), respectively. Arrows are represented to the changes and guided for eyes. (a) Changes in the O-H...O hydrogen-bonding distance ($d_{O...O}$, Å) between the free O atom of an axial H₂O ligand and a carboxylate group in F_xBA along the 1D chain. The $d_{O...O}$ distance at the HTP (filled symbol) is defined as $\Delta d \sim 0\%$. The ten, six, and five kinds of the independent $d_{O...O}$ were observed in crystals **1**, **2**, and **3**, respectively. (b) Schematic diagram of a definition of the dihedral angle (θ) between F_xBA ligands. (c) Change in the θ value with the phase transition temperature. The θ values in the HTP of crystals **1**, **2**, and **3** were expanded to ten, two, and eleven independent θ values in the LTP, respectively.

Structural transformation via phase transition: the origin of structural flexibility.

The DSC charts for crystals **1** and **3** showed the reversible phase transition peaks at 170.7 and 267.5 K, respectively (Figure S1 in Supporting Information). Although there was no evidence of first-order phase transition peaks in the DSC chart for crystal **2**, lowering of crystal symmetry was confirmed in an X-ray oscillation photograph at 170 K, due to the appearance of new Bragg diffractions, in contrast with those above 180 K (Figure S2). Therefore, all crystals exhibited temperature-dependent phase transition behavior. The crystallographic parameters above and below the phase transition temperature (T_{trs}) are summarized in Table 1. Although all the crystals showed no change in space group, the expansion of unit cell volumes (V) was observed from V at high temperature phase (HTP) to $5V$, $3V$, and $5V$ at low temperature phase (LTP) for crystals **1**, **2** and **3**, respectively (see Table 1 for details). The crystallographically independent $[\text{Cu}(\text{F}_x\text{BA})(\text{py})(\text{OH})]$ units in the HTP of crystals **1**, **2** and **3** were also enhanced to $5[\text{Cu}(4\text{-FBA})(\text{py})(\text{OH})]$, $3[\text{Cu}(3\text{-FBA})_2(\text{py})_2(\text{H}_2\text{O})]$, and $2.5[\text{Cu}(2,3\text{-F}_2\text{BA})_2(\text{py})_2(\text{H}_2\text{O})]$ units in the LTP, respectively (Figure S3-S5).

Figure 3a summarizes the amount of change (Δd , %) in the hydrogen-bonding $d_{O...O}$ distances between the O atom of a H₂O ligand and free O atoms of the carboxylate group in F_xBA. The uniform 1D hydrogen-bonding distances of $d_{O...O} = 2.772$, 2.808, and 2.760 Å in crystals **1**, **2** and **3**, respectively, were observed in the X-ray crystal structure analyses at the HTPs. On the contrary, one $d_{O...O}$ at the HTP underwent expansion or shrinkage to five $d_{O...O}(1) \sim d_{O...O}(5)$ lengths at the LTP in crystals **1**, **2** and **3** (details were summarized in Table S1 in ESI). The $\Delta d_{O...O}$ range from -3 to $+2\%$ at the LTP suggested the structural modulation of the O-H...O hydrogen-bonding 1D chain around the structural phase transition. The temperature-

the polar F_xBA ligands as the interchain correlation. To evaluate the interchain interactions, the θ value between the π -planes of the nearest neighboring F_xBA ligands (defined in Figure 3b) was evaluated at the HTP and LTP. The θ values at the HTP were $\theta = 0^\circ$ for **1**, $\theta = 28.16^\circ$ for **2**, and $\theta = 0^\circ$ and 38.74° for **3**. Although the θ values of crystal **2** at the LTP were almost independent of the temperature change, with $\theta = 27.79$ and 27.90° , change of the θ values for crystals **1** and **3** at the LTP were observed to be at the relatively wide angles of $\theta = 0$ – 43.02° and $\theta = 0$ – 36.3° , respectively, with a large modulation magnitude of $\Delta\theta \sim 40\%$ (Figure 3b). These large structural transformations at the LTP are due to the freezing of large-amplitude thermal fluctuations of dipoles in F_xBA ligands. The orientational disorder at the F atom of the 3,4-F₂BA ligand at the HTP in crystal **3** was also partially ordered at the LTP due to the freezing of the thermally activated molecular motions. The structural phase transitions of crystals **1** and **3** were consistent with the cooperative structural modulations of the 1D hydrogen-bonding chain and the orientation of polar F_xBA ligands. Only the modulation of the 1D hydrogen-bonding chain in crystal **2** showed no anomaly in the DSC trace.

Temperature- and frequency-dependent dielectric constants.

Figure 4 summarizes the temperature- and frequency-dependent real part of the dielectric constant (ϵ_1) using compressed pellets of crystal **3** in the cooling process. Data for crystals **1** and **2** are summarized in Figure S6. Although the slight dielectric anomalies around the T_{trs} were observed in the HTP–LTP boundaries of crystals **1** and **2**, the significant phase transition peaks in the dielectric constant were not confirmed in terms of the temperature dependence. Since the fluctuation of polar 4-FBA ligands along the C–COO[−] axis did not change the dipole moment of crystal **1**, there was almost no dielectric response upon changes in the temperature and frequency. The absence of the orientational disorder of 3-FBA ligands in the

crystal structure of **2** was also consistent with almost no dielectric response. On the contrary, enhancement of ϵ_1 was observed in crystal **3** upon increasing the temperature, suggesting the dynamic molecular motion of polar 3,4-F₂BA ligands. This enhancement from 240 K corresponded to the thermal anomaly seen in the DSC trace of crystal **3**. Frequency-dependent ϵ_1 enhancement was also observed for crystal **3**,

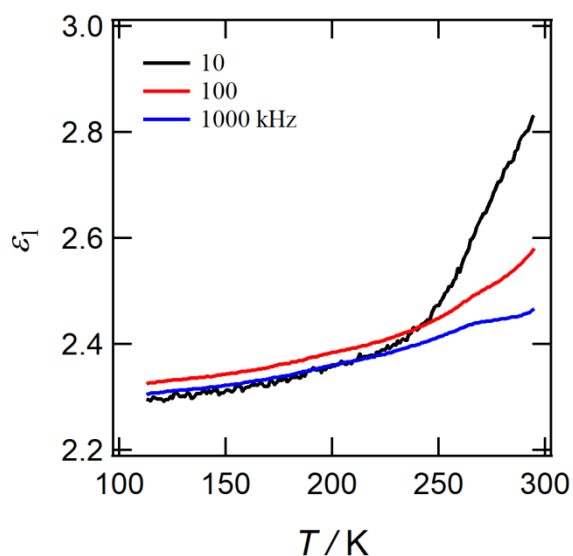


Figure 4. Temperature- and frequency-dependent real part of the dielectric constants (ϵ_1) for crystal **3** in the temperature range 100–300 K.

where ϵ_1 values reached the following values, suggesting the slow molecular motions of polar F_xBA ligands: $\epsilon_1 = 2.81$ for 10 kHz, $\epsilon_1 = 2.59$ for 100 kHz, and $\epsilon_1 = 2.48$ for 1000 kHz at 300 K.

Adiabatic heat capacity measurement.

The motional freedom in crystals is sensitive to the adiabatic molar heat capacity (C_p). Figure 5 summarizes the C_p of crystals **1**, **2**, and **3** in the temperature range 8–300 K. Table 2 summarizes the T_{trs} , the molar enthalpy ($\Delta_{\text{trs}}H$) and entropy ($\Delta_{\text{trs}}S$). The $\Delta_{\text{trs}}H = 0.7263 \pm 0.031$ kJ mol⁻¹ and $\Delta_{\text{trs}}S = 4.304 \pm 0.020$ J K⁻¹ mol⁻¹ for crystal **1** were approximately three times larger than the $\Delta_{\text{trs}}H = 0.2561 \pm 0.006$ kJ mol⁻¹ and $\Delta_{\text{trs}}S = 1.537 \pm 0.004$ J K⁻¹ mol⁻¹ for crystal **2**. The $\Delta_{\text{trs}}H = 1.569 \pm$

0.007 kJ mol⁻¹ and $\Delta_{\text{trs}}S = 6.078 \pm 0.025$ J K⁻¹ mol⁻¹ for crystal **3** were the highest among the three complexes. C_p anomalies were correlated to both the expansion and shrinkage of hydrogen bonds, and the molecular motion of F_xBA ligands, from structural analysis. The contributions to the C_p anomalies could, however, not be separated from other contributions, such as lattice vibration. The smallest magnitude of $\Delta_{\text{trs}}S$, in crystal **2**, was consistent with the structural modulation only in the 1D hydrogen-bonding chain in the absence of orientational changes of the polar ligands. The C_p anomalies also corresponded to the temperature- and frequency-dependent dielectric responses. The fluctuation of 4-FBA ligands in crystal **1** did not change the dipole moment and there was no effective ϵ_1 response around T_{trs} , whereas the ϵ_1 enhancement in crystal **3** originated from changes in the dipole moment due to the dipole fluctuation of polar 3,4-F₂BA ligands. Hence, the dipolar fluctuation of polar 3,4-F₂BA ligands affected the dielectric anomaly in crystal **3** upon the structural phase transition.

Table 2. Phase transition temperature (T_{trs}), molar enthalpy ($\Delta_{\text{trs}}H$), and molar entropy ($\Delta_{\text{trs}}S$), and molecular degree of freedom (w) for crystals **1**, **2**, and **3**

Crystal	1	2	3
$T_{\text{trs}} / \text{K}$	170.7	171.3	267.5
$\Delta_{\text{trs}}H / \text{kJ mol}^{-1}$	0.7263 ± 0.031	0.2561 ± 0.006	1.569 ± 0.007
$\Delta_{\text{trs}}S / \text{J K}^{-1} \text{mol}^{-1}$	4.304 ± 0.020	1.537 ± 0.004	6.078 ± 0.025

Conclusions

Structural flexibility coupled with intermolecular hydrogen-bonding and dipole–dipole interactions indicated structural phase transition accompanied with dipole fluctuation. Three Cu^{II} complexes, [Cu^{II}(4-FBA)₂(pyridine)₂(H₂O)] (**1**), [Cu^{II}(3-FBA)₂(pyridine)₂(H₂O)] (**2**), and [Cu^{II}(3,4-F₂BA)₂(pyridine)₂(H₂O)] (**3**) (where 4-FBA = 4-fluorobenzoate, 3-FBA = 3-fluorobenzoate, and 3,4-F₂BA = 3,4-difluorobenzoate) formed the 1D O–H•••O hydrogen-bonding chains and their 3D assembly structures through weak dipole–dipole interaction at polar fluorinated benzoate (F_xBA) ligands. Three crystals showed phase transition behavior associated with structural modulations of the 1D hydrogen-bonding chain and the

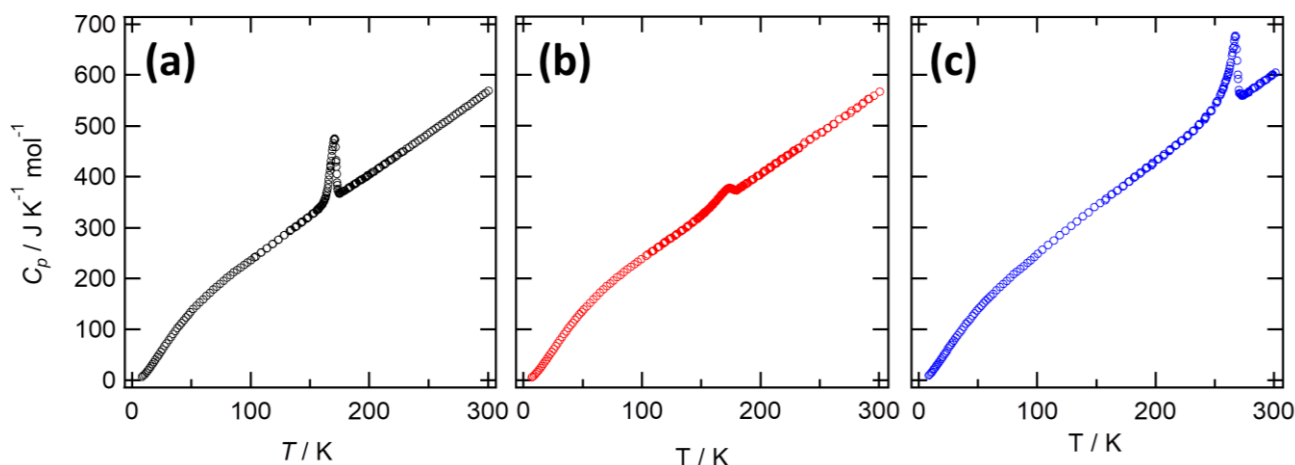


Figure 5. Adiabatic molar heat capacity of crystals in the temperature range 8–300 K: (a) **1**, (b) **2**, and (c) **3**.

orientational changes of the polar ligands upon heating. In particular, large-amplitude molecular motions of polar 4-FBA and 3,4-F₂BA ligands was observed in crystals **1** and **3** around the phase transition temperatures, as reflected in the results of DSC, dielectric response, and molar heat capacity. Cooperative modulation of the intermolecular hydrogen-bonding and dipole–dipole interactions is a driving force of the phase transition and also ligand rearrangements. Further designs methods for structural flexibility, coupled with weak intermolecular interactions, offer a synergetic effect toward the fabrication of dynamic molecular systems.

Conflicts of interest

There are no conflicts to declare.

Acknowledgements

This work was supported by a Grant-in-Aid for Science Research from the Ministry of Education, Culture, Sports, Science, and Technology (MEXT) of Japan, and by Management Expenses Grants for National Universities of Japan and Grant-in-Aid for Early-Career Scientists (JP21K14691), Kiban Kenkyu (B) (JP18H01949), Scientific Research on Innovative Areas ‘ π -Figuration’ (JP26102007), Kiban Kenkyu (A) (JP19H00886), JST CREST Grant Number JPMJCR18I4, “Dynamic Alliance for Open Innovation Bridging Human, Environment and Materials” from MEXT, and “Dynamic Alliance for Young Researcher” from the Research Institute for Electronic Science, Hokkaido University.

Notes and references

- G. R. Desiraju, J. J. Vittal and A. Ramanan, *Crystal engineering: a textbook*, World Scientific, 2011.
- C. Wang, H. Dong, L. Jiang and W. Hu, *Chem. Soc. Rev.*, 2018, **47**, 422–500.
- K. Heuzé, C. Mézière, M. Fourmigué, P. Batail, C. Coulon, E. Canadell, P. Auban-Senzier and D. Jérôme, *Chem. Mater.*, 2000, **12**, 1898–1904.
- H. Jiang, P. Hu, J. Ye, K. K. Zhang, Y. Long, W. Hu and C. Kloc, *J. Mater. Chem. C*, 2018, **6**, 1884–1902.
- L. Su, W. C. Song, J. P. Zhao and F. C. Liu, *Chem. Commun.*, 2016, **52**, 8722–8725.
- G. Bolla, H. Dong, Y. Zhen, Z. Wang and W. Hu, *Sci. China Mater.*, 2016, **59**, 523–530.
- O. König, H. B. Bürgi, T. Armbruster, J. Hulliger and T. Weber, *J. Am. Chem. Soc.*, 1997, **119**, 10632–10640.
- O. Sato, *Nat. Chem.*, 2016, **8**, 644–656.
- T. Akutagawa, *Bull. Chem. Soc. Jpn.*, 2021, **94**, 1400–1420.
- T. Akutagawa, *Mater. Chem. Front.*, 2018, **2**, 1064–1073.
- T. Akutagawa, H. Koshinaka, D. Sato, S. Takeda, S.-I. Noro, H. Takahashi, R. Kumai, Y. Tokura and T. Nakamura, *Nat. Mater.*, 2009, **8**, 342–347.
- S. L. Gould, D. Tranchemontagne, O. M. Yaghi and M. A. Garcia-Garibay, *J. Am. Chem. Soc.*, 2008, **130**, 3246–3247.
- I. Hisaki, N. Ikenaka, S. Tsuzuki and N. Tohnai, *Mater. Chem. Front.*, 2018, **2**, 338–346.
- I. Hisaki, Q. Ji, K. Takahashi, N. Tohnai and T. Nakamura, *Cryst. Growth Des.*, 2020, **20**, 3190–3198.
- K. Takahashi, N. Hoshino, T. Takeda, K. Satomi, Y. Suzuki, S. Noro, T. Nakamura, J. Kawamata and T. Akutagawa, *Dalt. Trans.*, 2016, **45**, 3398–3406.
- Y. Kume, Y. Mlyazaki, T. Matsuo and H. Suga, *J. Phys. Chem. Solids*, 1992, **53**, 1297–1304.
- O. V Dolomanov, L. J. Bourhis, R. J. Gildea, J. A. K. Howard and H. Puschmann, *J. Appl. Crystallogr.*, 2009, **42**, 339–341.
- M. C. Burla, R. Caliandro, M. Camalli, B. Carrozzini, G. L. Cascarano, L. De Caro, C. Giacovazzo, G. Polidori and R. Spagna, *J. Appl. Crystallogr.*, 2005, **38**, 381–388.
- M. C. Burla, R. Caliandro, M. Camalli, B. Carrozzini, G. L. Cascarano, C. Giacovazzo, M. Mallamo, A. Mazzone, G. Polidori and R. Spagna, *J. Appl. Crystallogr.*, 2012, **45**, 357–361.
- G. M. Sheldrick, *Acta Crystallogr. Sect. A Found. Adv.*, 2015, **71**, 3–8.
- G. M. Sheldrick, *Acta Crystallogr. Sect. C Struct. Chem.*, 2015, **71**, 3–8.